Moiré interferometry for engineering mechanics: current practices and future developments

B HAN[1*], **D Post**[2] and **P Ifju**[3]

[1] Mechanical Engineering Department, University of Maryland, College Park, Maryland, USA
[2] Department of Engineering Science and Mechanics, Virginia Polytechnic Institute and State University, Blacksburg, Virginia, USA
[3] Aerospace Engineering, Mechanics and Engineering Science, University of Florida, Florida, USA

Abstract: In the past decade, the optical method called moiré interferometry has matured rapidly to emerge as an invaluable tool, proved by many industrial and scientific applications. It has been applied to numerous problems in engineering mechanics. It measures in-plane displacement fields with high sensitivity and high spatial resolution. This paper reviews current practices of moiré interferometry and its extensions. Diverse applications are referenced to emphasize the wide scope of the method in engineering mechanics. Examples in the text are from the microelectronics industry, where moiré interferometry is used extensively for experimental analyses of temperature-induced deformations. In-depth speculation on future developments and practices is presented.

Keywords: moiré interferometry, engineering mechanics

1 INTRODUCTION

Today, moiré interferometry is used for many studies [1]. It has been applied for studies of composite materials [2-18], polycrystalline materials [1, 19], piezoelectric materials [20], fracture mechanics [21-28], biomechanics [29], structural elements [30,31], structural joints [32-35], residual stress measurement [36-42], and strain gage calibration [1,43]. More recently, it has been practiced extensively in the microelectronics industry to measure thermally induced deformation of electronic packages [44-59].

Moiré interferometry measures in-plane displacements with a very high sensitivity. The data are received as interference fringe patterns, or contour maps, of the displacement fields. Because of the high sensitivity and abundance of data, reliable strain distributions (normal strains and shear strains) can be extracted from the patterns. The method differs from classical interferometry and holographic interferometry, which are most effective for measuring out-of-plane displacements.

Moiré interferometry is characterized by a list of excellent qualities, including the following:

(a) full-field technique, i.e. quantitative measurements can be made throughout the field;
(b) high sensitivity to in-plane displacements U and V, typically 0.417 μm per fringe order, but extended to 17 nm per fringe contour by microscopic moiré interferometry;
(c) insensitive to out-of-plane displacements W;
(d) high spatial resolution, which means that measurements can be made in tiny zones;
(e) high signal-to-noise ratio, ensuring that the fringe patterns have high contrast and excellent visibility;
(f) large dynamic range, providing a method that is compatible with large and small displacements, large and small strains, large and small strain gradients; there are no correlation requirements;
(g) determination of shear strains as readily as normal strains;
(h) real-time technique—the displacement fields can be viewed as loads are applied

Reference [1] provides comprehensive coverage of the theory and practice, and diverse applications of moiré interferometry in one volume. Additional technical information can be found in the recent literature by Patorski [60], Cloud [61], and others. This paper is intended to describe the qualities and basic concepts of moiré interferometry, to present some current applications, and to speculate on future developments and practices. Although the literature reports applications in many diverse fields, the applications described here are from the microelectronics

The MS was received on 11 May 2000 and was accepted after revision for publication on 5 September 2000.
[*]Corresponding author: Glenn L. Martin Institute of Technology, Department of Mechanical Engineering, University of Maryland, 2181 Glenn L. Martin Hall, College Park, MD 20742-3035, USA

industry. These represent a broad spectrum of problems and experimental solutions, which give insight into the potential of moiré interferometry for other fields of study.

2 METHOD

2.1 Basic Concept

The general scheme of moiré interferometry is illustrated in Fig. 1. A high-frequency cross-line grating on the specimen, initially of frequency f_s, deforms together with the specimen. A parallel (collimated) beam, B_1, of laser light strikes the specimen and a portion is diffracted back, nominally perpendicular to the specimen, in the +1 diffraction order of the specimen grating. Light from the mutually coherent collimated beam B_2 is diffracted back in its -1 order. Since the specimen grating is deformed as a result of the applied loads, these diffracted beams are no longer collimated. Instead, they are beams with warped wavefronts, where the warpages are related to the deformation of the grating. These two coherent beams interfere in the image plane of the camera lens, producing an interference pattern of dark and light bands, which is the N_x moiré pattern.

Similarly, mutually coherent collimated beams B_3 and B_4, centered in the vertical plane, are diffracted in +1 and -1 diffraction orders by the nominally horizontal lines of the deformed specimen grating. These two diffracted beams interfere to produce the N_y moiré pattern. In practice, beams B_1 and B_2 are blocked, so the N_y fringes are viewed alone. Alternately, B_3 and B_4 are blocked to view the N_x fringes.

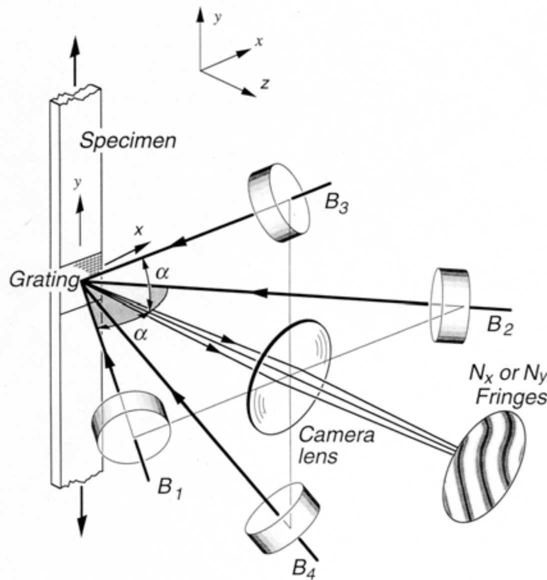

Fig. 1 Schematic illustration of four-beam moiré interferometry to record the N_x and N_y fringe patterns, which depict the U and V displacement fields [1]

These moiré patterns are contour maps of the U and V displacement fields, i.e., the displacements in the x and y directions, respectively, of each point in the specimen grating. The relationships, for every x,y point in the field of view, are

$$U(x,y) = \frac{1}{2f_s} N_x(x,y)$$
$$V(x,y) = \frac{1}{2f_s} N_y(x,y) \tag{1}$$

In routine practice of moiré interferometry, f_s = 1200 lines/mm (30,480 lines/in.). In the fringe patterns, the contour interval is $1/2f_s$, which is 0.417 μm displacement per fringe order. The sensitivity is its reciprocal, 2.4 fringes per μm displacement. For microscopic moiré interferometry, described later, sensitivity of 57.6 fringe contours per μm displacement has been achieved.

The basis of moiré interferometry is described above by this sequence:

1. Two beams are incident upon the specimen grating.
2. Diffraction of each beam by the deformed grating produces two warped wavefronts emerging from the specimen.
3. The coherent addition of these two beams produces the moiré pattern by constructive and destructive interference.

This is an excellent physical explanation. It is consistent with the mathematical derivation, which defines the intensity distribution in the moiré pattern and its relationship, equation (1) to the fringe orders [1].

However, another physical explanation is equally compelling; perhaps it is more closely related to our experience and intuition, and perhaps it is more helpful for understanding the relationship between the deformation and the moiré pattern. It is very simple.

Figure 2a illustrates unobstructed beams B_1 and B_2 in a two-dimensional cross-sectional view. Assuming the two beams have propagated equal distances from the source to point a, constructive interference occurs along the plane of symmetry, ab. The path lengths between the source and any point in this plane are equal for the two beams. Along an adjacent plane, the path lengths of B_1 and B_2 differ by $\lambda/2$ at every point, so destructive interference, or the absence of light, occurs in that plane. Along another adjacent plane, the path difference is λ, creating a plane of constructive interference, etc. Accordingly, the volume of space where beams B_1 and B_2 coexist is filled with a regular array of planes of constructive interference, alternating with planes of destructive interference. These represent bright

 S03000 © IMechE 2001

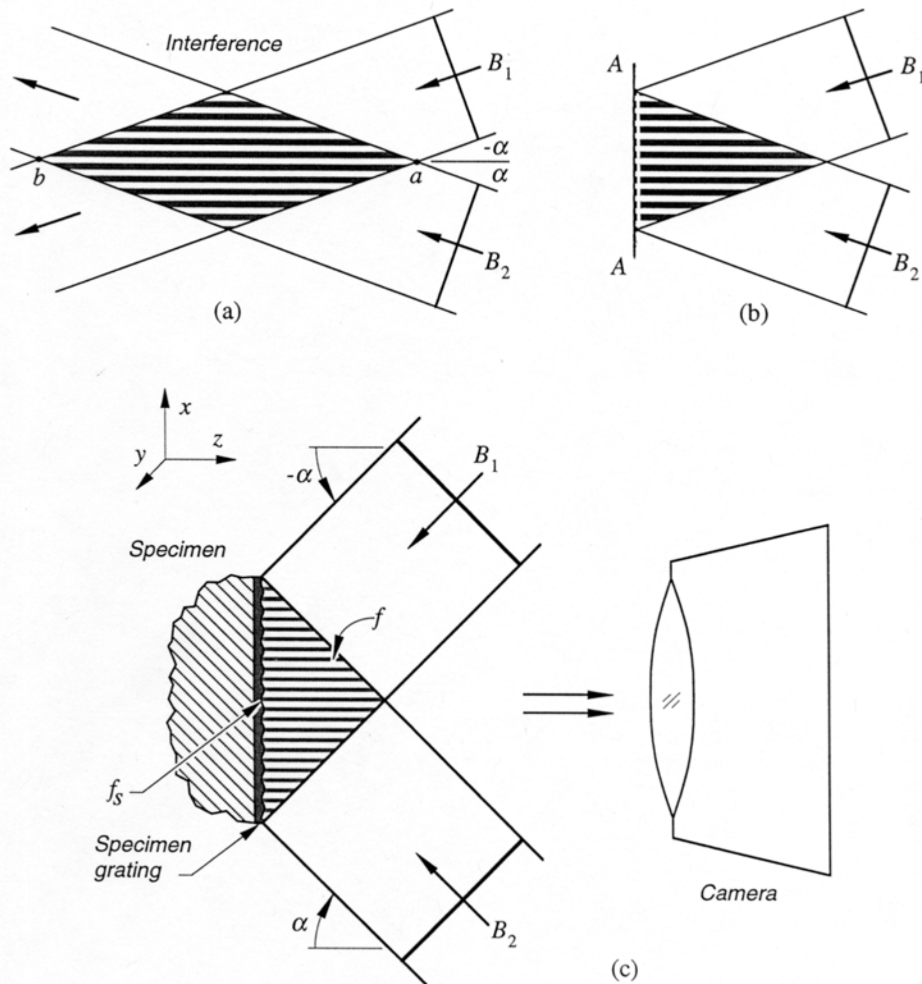

Fig. 2 Schematic diagrams illustrating (a) constructive and destructive interference at the intersection of two coherent beams, (b) a virtual reference grating on plane AA and (c) the interaction of a virtual reference grating and a specimen grating, which creates a moiré pattern [1]

regions of light separated by regions of darkness. The volume of space is said to be filled with *walls of interference*.

In Fig. 2b, the walls are cut by plane *AA*, which becomes illuminated by an array of bright bands, separated by dark bands. The illumination resembles a bar-and-space grating, and it is fully analogous to the reference grating of geometrical moiré. In moiré interferometry, it functions as a reference grating. There is no physical reference grating in moiré interferometry, but the two incident beams create a *virtual reference grating*. The volume of space where the two beams coexist is called a *virtual grating* and the array of bright and dark bands that illuminates the specimen is called a virtual reference grating.

In the second physical description of moiré interferometry, the virtual reference grating and the deformed specimen grating interact to form the moiré pattern, which is recorded by a camera. The system is illustrated in Fig. 2c. The effect is analogous to geometrical moiré, but since it is proved that the equations of moiré interferometry and geometrical moiré are identical [62], the description is fully justified.

The frequency, f, of the virtual reference grating is determined by the angle α and wavelength λ by

$$f = \frac{2}{\lambda}\sin\alpha \tag{2}$$

For the usual applications, f = 2400 lines/mm (60,960 lines/in.). Moiré interferometry utilizes a virtual reference grating of twice the initial frequency of the specimen grating, i.e.,

$$f = 2f_s \tag{3}$$

This corresponds to moiré fringe multiplication by a factor of 2. The resulting sensitivity is determined by the

reference grating, corresponding to geometrical moiré with gratings of frequency *f*.

Again, the second physical explanation is consistent with the mathematical derivation, in which the intensity distribution in the moiré pattern, and also equation (1) are derived [1]. Fringe order N_x determines the in-plane displacements U at each point in the field, uniquely; although the specimen and specimen grating experiences V and W displacements (where W is the out-of-plane displacement), the N_x pattern is a simple function of U, alone. Similarly, the mathematical derivation proves that the N_y pattern is a function of V, independent of U and W.

2.2 Optical Configurations

Any configuration of optical and mechanical components that produces the four beams illustrated in Fig. 1 can be used. Of course, each pair of beams must be mutually coherent. Several configurations are illustrated and described in reference [1]. Fine adjustments of beam direction are required to control precisely the initial null field and, when desired, the carrier fringes. An extremely important feature is robust construction to minimize sensitivity to external disturbances, primarily vibrations from mechanical and acoustical sources, and secondarily, air currents and thermal disturbances. Compact construction is an asset in this regard [63]. Commercial moiré systems based on various optical arrangements have been introduced in the marketplace and numerous systems have been put into practice in industry and at university and government laboratories.

2.3 Extension: Microscopic Moiré Interferometry

Special considerations arise for deformation measurements of tiny specimens or tiny regions of larger specimens. The relative displacements within a small field of view will be small (even if the strains are not small); thus the number of moiré fringes might not be enough for an accurate analysis. Perhaps the most important consideration, therefore, is the need for increased displacement sensitivity–enhanced sensitivity beyond the high sensitivity discussed above.

In a method called *microscopic moiré interferometry*, sensitivity is increased progressively by two techniques. The first is an *immersion interferometer*, whereby the virtual reference grating is formed inside a medium of higher index of refraction; this strategy reduces the wavelength of the light and thus increases the upper limit of frequency for the virtual reference grating. Virtual reference gratings of 4800 lines/mm (122,000 lines/in.) are produced in practice, thus doubling the usual basic sensitivity [64]. The second technique is optical/digital fringe multiplication (O/DFM), whereby fringe shifting and an efficient algorithm is used to generate an enhanced contour map of the displacement field; the map displays β times as many fringe contours as the original moiré pattern [65]. In practice, $\beta = 12$ has been achieved for microscopic moiré interferometry, which with the doubled sensitivity, represents a multiplication of 24.

A specific system is described briefly. It has been described in much more detail in reference [1] and [66]. The technique is based on the premise that the moiré pattern encompassing the small field of view will contain only a few fringes. Accordingly, it is practical to record the pattern by a charge-coupled device (CCD) camera. Good fringe resolution is preserved because the pattern is recorded with numerous pixels per fringe.

The apparatus is illustrated in Fig. 3. The specimen is coupled optically to the interferometer by a thin layer of immersion fluid, so that beams corresponding to B_1—B_4 in Fig. 1 propagate in a refractive medium. A magnified view of the fringe pattern is recorded by the CCD camera, which digitizes the intensity level at every pixel. A piezoelectric translation device provides the means for phase stepping. The entire system is moved relative to the specimen by the *xy* traverse, allowing any part of the specimen to be viewed and analyzed.

2.4 Specimen Gratings

The bar-and-space gratings of geometrical moiré cannot be printed with very high frequencies. Instead, phase gratings are used, which means that the grating surface consists of a regular array of hills and valleys. For most analyses, the specimen grating is applied by the replication process illustrated by cross-sectional views in Fig. 4. A special mold is used, which is a plate with a cross-line phase grating on its surface. The grating is overcoated with a highly reflective metallic film, usually evaporated aluminum. A small pool of liquid adhesive is poured on the mould, and the specimen is pressed into the pool to spread the adhesive into a thin film. Excess adhesive is cleaned off repeatedly as it flows out. The mold is pried off after the adhesive has hardened. The weakest interface is between the metallic film and the cross-line grating, so the film is transferred to the specimen. Thus, a thin, highly

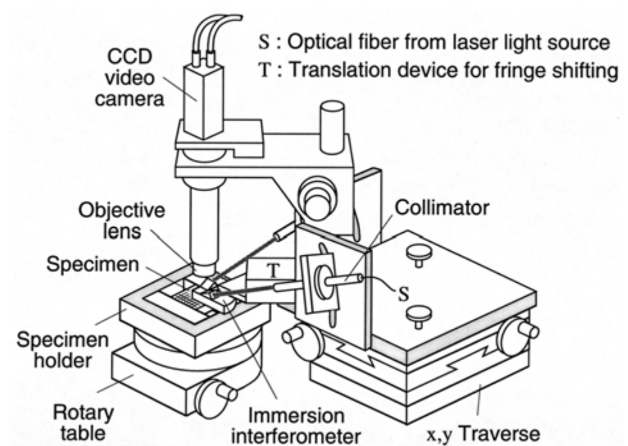

Fig. 3 Mechanical and optical arrangement for microscopic moiré interferometry [66]

 S03000 © IMechE 2001

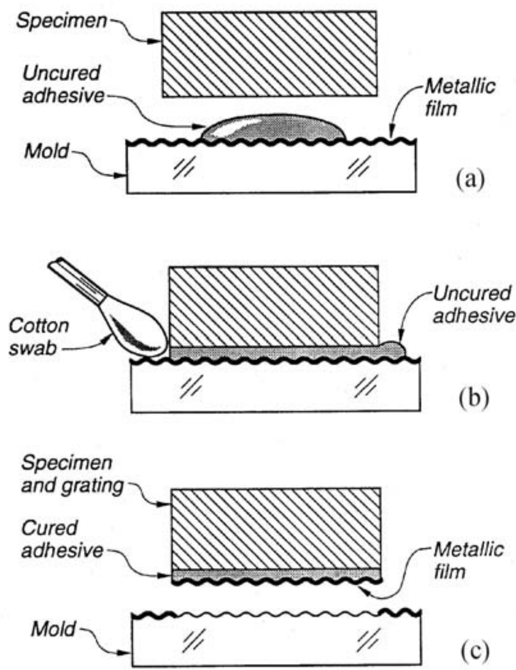

Fig. 4 Steps in producing the specimen grating by a casting or replication process; the reflective metallic film is transferred to the specimen grating [1]

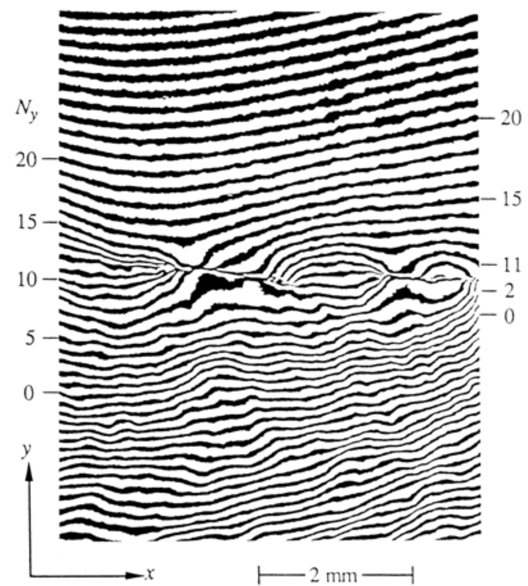

Fig. 5 Weld defects in a stainless steel tension specimen [33]. (Reproduced by permission of S.A. Chavez)

reflective cross-line grating is firmly attached to the specimen surface, such that it deforms together with the specimen surface. Details can be found in Chapter 4 and Appendix C of reference [1].

The adhesive thickness is typically about 25 μm (0.001 in.) for larger specimens (greater than 300 mm^2) and about 2 μm for small specimens. For most analyses the thickness and stiffness of the grating is negligible. Various room temperature curing adhesives can be used, including epoxies, acrylics, urethanes, and silicone rubbers. Recent reports of success with instant cyanoacrylate cements have been circulated. Adhesives that cure by exposure to ultraviolet light have been used successfully. Special techniques have been developed for replicating specimen gratings on electronic packages, to cope with the small size and tiny openings [47,49], as discussed later.

2.5 Fringe Counting

The assignment of fringe orders has been treated in more detail in reference [1]. Because deformations are determined by the relative displacements of each point in a body, the zero-order fringe is arbitrary; the zeroth order can be assigned to any fringe in the moiré pattern. In Fig. 5, it is assigned in the lower left region of the specimen. Of course, at every point along this continuous fringe, $N_y = 0$.

Figure 5 shows the deformation of a tensile coupon cut from a stainless steel plate in the region of a weld [33]. Cracks appear in the weld, but along the left edge of the specimen the material is continuous. Since the strain is tensile, or positive, the fringe orders along the left edge increase monotonically in the +*y* direction, as shown. Then the fringe orders can be assigned at every point in the field by following continuous fringes across the field. Fringe orders along the right edges were assigned accordingly.

Where a crack is present, the *V* displacements are different along the upper and lower lips of the crack. This accounts for the crack opening that results from the tensile load. For example, at the right edge the fringe order changes from $N_y = 3$ to $N_y = 10$, indicating a crack-opening displacement of 7 fringe orders, or 2.9 μm.

Clues derived from known loading conditions and known specimen geometry are often sufficient to establish the sign of the fringe gradient at every point, i.e., to establish whether the fringe order is increasing or decreasing as the count progresses from one fringe to the next neighboring fringe. Occasionally the clues might not be sufficient, but there is always a simple experimental way to determine the sign of the fringe gradient [1].

2.6 Strain Analysis

Strains can be determined from the two displacement fields by the relationships for engineering strain:

$$\varepsilon_x = \frac{\partial U}{\partial x} = \frac{1}{f}\left[\frac{\partial N_x}{\partial x}\right],\ \varepsilon_y = \frac{\partial V}{\partial y} = \frac{1}{f}\left[\frac{\partial N_y}{\partial y}\right] \qquad (4)$$

$$\gamma_{xy} = \frac{\partial U}{\partial y} + \frac{\partial V}{\partial x} = \frac{1}{f}\left[\frac{\partial N_x}{\partial y} + \frac{\partial N_y}{\partial x}\right] \qquad (5)$$

where ε is the normal strain and γ is the shear strain at the surface of the specimen. Although it is not indicated here by the (*x,y*) suffix [shown in equation (1)], these equations apply for every point in the field. Thus, it is the fringe

gradients that determine the strains, both the normal strains and the shear strains.

In principle, the exact differential can be extracted at any point by plotting a curve of fringe orders along a line through the point and measuring the slope of the curve at the point. Often, however, the finite increment approximation is sufficient, whereby (as an example) $\partial N_x/\partial x$ is taken to be equal to $\Delta N_x/\Delta x$. In that case, strain is determined by measuring Δx, the distance between neighboring fringes, in the immediate neighborhood of the point of interest.

Shear strains are determined as readily as normal strains. Numerous examples of fringe counting and strain analysis are given in reference [1]. In nearly all cases of strain analysis, the strains are sought at specific points (e.g., where the fringes are most closely packed, indicating strain maxima), or along specific lines. Manual methods, and computer-assisted methods are most practical for such cases.

3 SELECTED APPLICATIONS FOR MICROELECTRONICS DEVICES

Microelectronics devices contain many electronic components within an active silicon chip, such as transistors, capacitors, resistors, etc. To form a usable device, a silicon chip requires protection from the environment as well as electrical and mechanical connections to the surrounding components. The various conducting and insulating materials involved in the devices have different coefficients of thermal expansions (CTE). When electrical power is applied, the device is subjected to a temperature excursion and each material expands at a different rate. This non-uniform CTE produces thermally induced mechanical stresses within the device assembly.

As the components and structures involved in high-end microelectronics devices are made smaller, the thermal gradient increases and the strain concentrations become more serious. Hence, there is a continuously increasing activity in experimental analysis, both for specific studies and for guidance of numerical analyses. Moiré interferometry is taking a leadership role for experimental analyses. A few diverse applications are presented here.

3.1 Grating Replication for Complex Geometry

A special technique is required for replicating a specimen grating on the cross sections of microelectronics devices because they usually have such a tiny and complex geometry that the excess epoxy produced by the grating replication procedure shown in Fig. 4 cannot be swabbed away. The excess epoxy is critical since it could reinforce the specimen and change the local strain distribution.

An effective replication technique was developed to circumvent the problem [47,49]. First, a tiny amount of liquid epoxy is dropped onto the grating mould; the viscosity of the epoxy should be extremely low at the replication temperature. Then, a lintless optical tissue (a lens tissue) is dragged over the surface of the mold, as illustrated in Fig. 6. The tissue spreads the epoxy to produce a very thin layer of epoxy on the mould. The specimen is pressed gently into the epoxy, and it is pried off after the epoxy has polymerized. Before polymerization, the surface tension of the epoxy pulls the excess epoxy away from the edges of the specimen. The result is a specimen grating with a very clean edge. The specimen must be made very flat and smooth to be compatible with the thin film of epoxy. The thickness of specimen gratings produced by this procedure is about 2 μm.

3.2 Bithermal Loading (Isothermal Loading)

Thermal deformations can be analyzed by room temperature observations. In this technique, the specimen grating is applied at an elevated temperature, and it is allowed to cool to room temperature before it is observed in the moiré interferometer. Thus, the deformation incurred by the temperature increment is locked into the grating and recorded at room temperature [1,67].

A typical temperature increment is 80°C, whereby the grating is applied at about 100°C and observed at about 20°C. An adhesive that cures at elevated temperature is used, usually an epoxy. The specimen and mould are pre-heated to the application temperature, the adhesive is applied, and it is allowed to cure at the elevated temperature. The mould is a grating on an ultra-low expansion (ULE) substrate; so its frequency is the same at elevated and room temperatures. Otherwise, a correction is required for the thermal expansion of the mould.

These measurements can be achieved for cryogenic

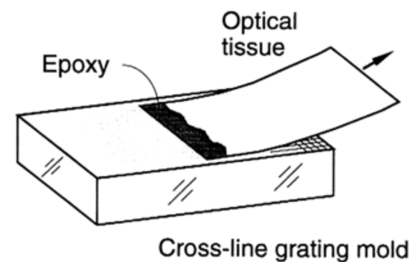

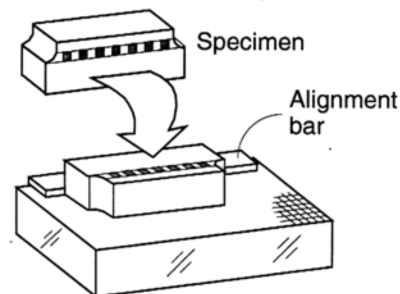

Fig. 6 Procedure to replicate a specimen grating on a specimen with a complex geometry

temperatures, too. In one test, the specimen grating was applied at -40°C using an adhesive that cured in ultraviolet light [1].

This technique had come to be known as *isothermal loading* in recent years, but that name implies constant temperature and therefore it is not descriptive. The present authors propose to call the technique *bithermal loading*, implying two discrete temperatures.

3.3 Bithermal Loading: Flip-Chip Plastic Ball Grid Array Package Assembly

An example of bithermal loading is illustrated in Fig. 7 [54]. The specimen is a flip-chip plastic ball grid array (FC-PBGA) package assembly. In the assembly, a silicon chip (6.8 mm x 6.1 mm x 1.2 mm) was first attached to an organic substrate through tiny solder bumps. The gap between the chip and the substrate was filled with an epoxy underfill to help resist the thermal stresses induced in the solder bumps. This subassembly was then surface-mounted to a typical FR-4 printed circuit board (PCB) through larger solder ball arrays to form a final assembly. The assembly was cut and its cross-section was ground to produce a flat, smooth, cross-sectional surface. The specimen grating was replicated at 82°C and the fringes were recorded at room temperature (ΔT = -60°C). Very clean edges of the specimen grating are evident.

The V field fringe pattern reveals the detailed bending deformation of the substrate. The vertical displacements along the centerlines of the substrate and the PCB were determined from the fringe patterns and they are plotted in Fig. 8a. Two distinct curvatures are observed, one in the area connected to the chip and the other in the rest of the substrate. The CTE of the substrate was higher than that of the PCB. The substrate contracted more than the PCB during cooling, while the deformation of the substrate covered by the chip was constrained by the low CTE of the chip. This complicated loading condition produced an uneven curvature of the substrate, which resulted in an inflection point below the edge of the chip.

The substrate was connected to the PCB through the solder balls and the difference of curvature between the substrate and the PCB was accommodated by the deformation of the solder balls. The normal and shear strains (averaged along the vertical center-line) at each solder ball were calculated from the fringe patterns and they are plotted in Fig. 8b. The largest of these normal strains occurred in the solder ball located at the edge of the chip and its magnitude was nearly four times greater than the largest shear strain. Although symmetry about the central solder ball would be expected, the small deviations from precise symmetry are characteristic of real structures.

This result is entirely different from the results of a previous study on a ceramic ball grid array (CBGA) package assembly [49]. The subsequent numerical parametric study quantified the effect of the substrate CTE on the solder ball strains. The study indicated that the substrate CTE was one of the most critical design parameters for optimum solder joint reliability [54]. The experimental evidence provided by moiré interferometry was essential to revealing this important design parameter.

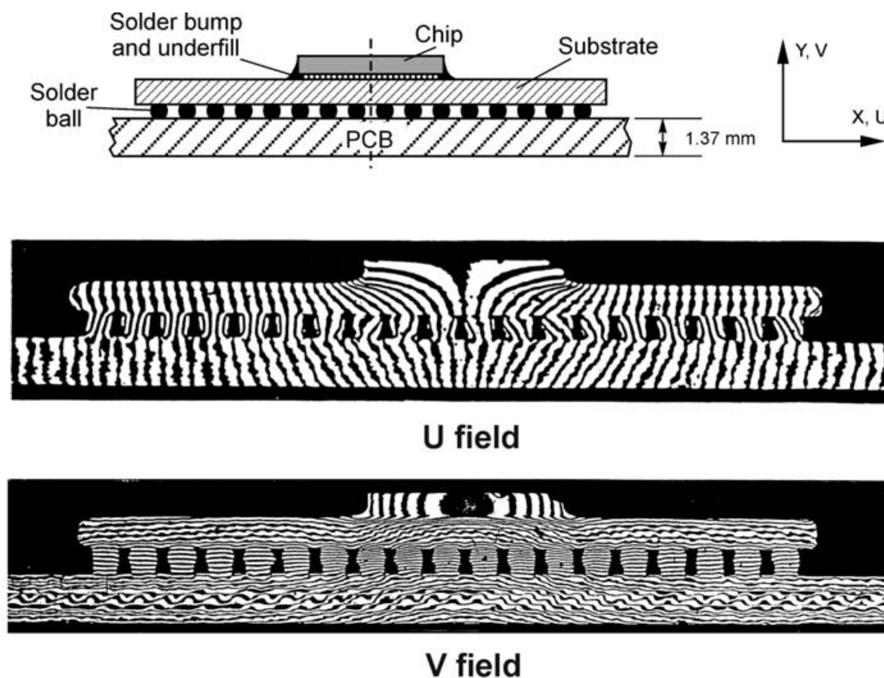

Fig. 7 ***U* and *V* displacement fields of an FC-PBGA package assembly, induced by thermal loading of ΔT = -60 °C [54]. The contour interval is 0.417 μm per fringe**

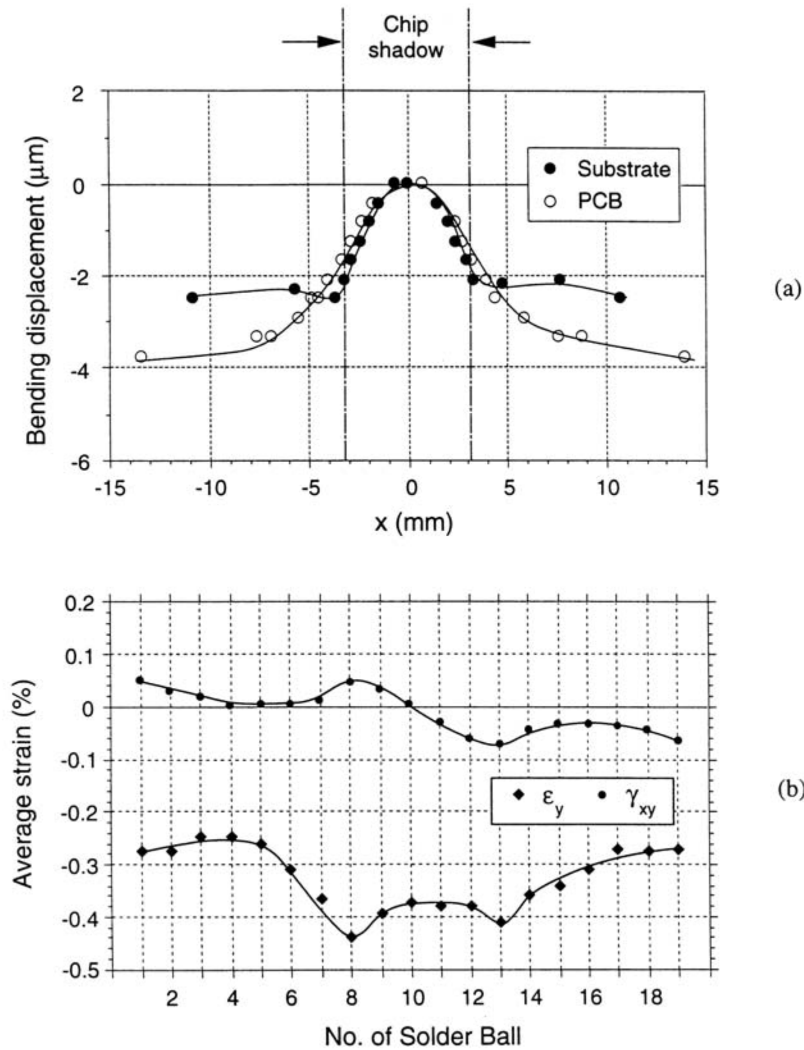

Fig. 8 (a) Vertical displacements determined along the centre-lines of the substrate and the PCB and (b) distribution of normal and shear strains (averaged along the vertical centre-line) at each solder ball

3.4 Accumulated Inelastic Deformation: Ceramic Column Grid Array Package Assembly

The effect of thermal cycling on solder columns was investigated [55]. The ceramic column grid array (CCGA) package is an extension of the CBGA package but it offers enhanced solder joint fatigue reliability through a compliant solder column. The specimen was a CCGA package assembled to an FR-4 PCB. The CCGA package was a 44 mm square module with 1089 input-output interconnections (33 by 33). A schematic diagram of the column assembly is shown in Fig. 9a with relevant dimensions. The assembly contained cast-in-place columns, where wire solder columns were cast directly on the ceramic module and subsequently connected to a PCB using eutectic solder. The wire solder column is made of a high-melting point solder alloy (90%Pb/10%Sn). The wire column does not melt during the assembly process, which provides a consistent and reproducible standoff between the ceramic package and the PCB.

One side of the specimen was ground flat to expose the largest cross section of solder columns for specimen grating replication. The procedure of bithermal loading (ΔT = -60°C) was used first to document the deformation induced by an initial thermal loading simulating the assembly process. The U and V displacement fields are shown in Fig. 9b for the end column, i.e. the column most distant from the center. The deformation of the solder column was dominated by bending (flexure), as revealed by nearly zero shear strains at the middle of the column.

The same specimen was subjected to subsequent thermal cycles. The maximum and minimum temperature in

 S03000 © IMechE 2001

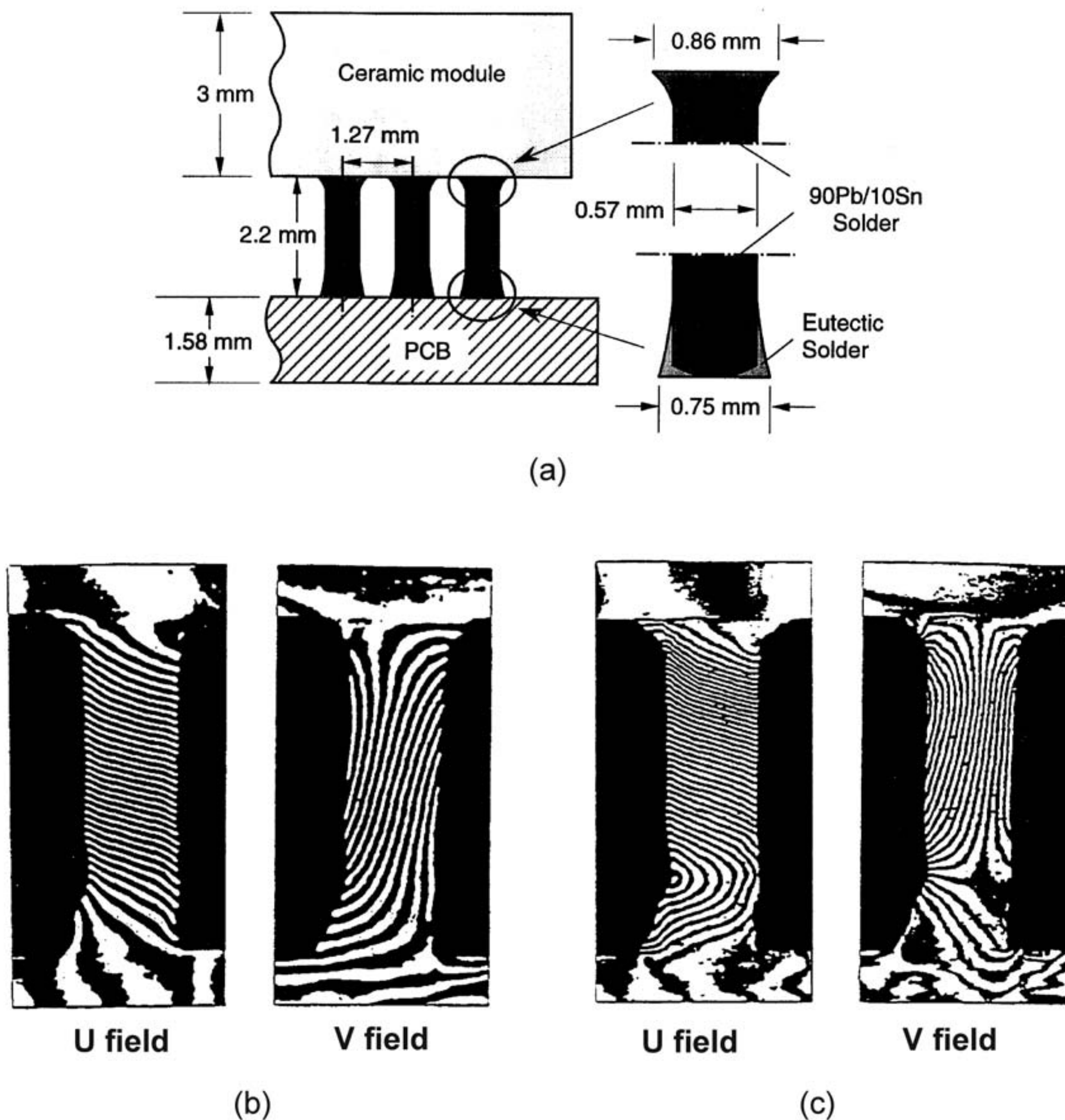

Fig. 9 (a) Schematic diagram of a CCGA assembly. (b), (c) U and V displacement fields, induced by (b) initial thermal loading and (c) four subsequent thermal cycles of -40 to 125°C [55]. The contour interval is 0.417 mm per fringe

the cycle was 125°C and -40°C. The heating and the cooling rate was 16.5°C/minute and a dwell time of 5 min was used at each extreme temperature, which resulted in a period of 30 minutes per cycle. The total U and V displacements of the same column after four complete thermal cycles are shown in Fig. 9c.

The fringe patterns in Fig. 9 were used to determine the deformed shape of the column. The fringe patterns were marked at uniform intervals along the boundary and the (fractional) fringe orders were determined at each mark. Then, the deformed shape was plotted by displacing each boundary point by an amount proportional to the U and V fringe orders. The results are shown in Fig. 10a for the initial bithermal loading and Fig. 10b after four thermal cycles, where the deformations were greatly exaggerated.

It is interesting to note that while the relative horizontal displacement between P1 and P3 are nearly the same, the deformed shapes are quite different around the region with the eutectic solder fillet. Eutectic solder has a much lower melting point and thus it is more susceptible to deformation at the elevated temperature during the thermal cycles (smaller Young's modulus and higher creep rate), compared with the high-melting solder. The creep of eutectic solder was much greater during the high temperature interval and this deformation accumulated during the thermal cycles. As a result, the lower portion of the column, surrounded by the eutectic solder, remained bent in the opposite direction and it could not return to its previous geometry at room temperature. This effect was confirmed by the results from an actual accelerated thermal cycling (ATC) test [55]. The

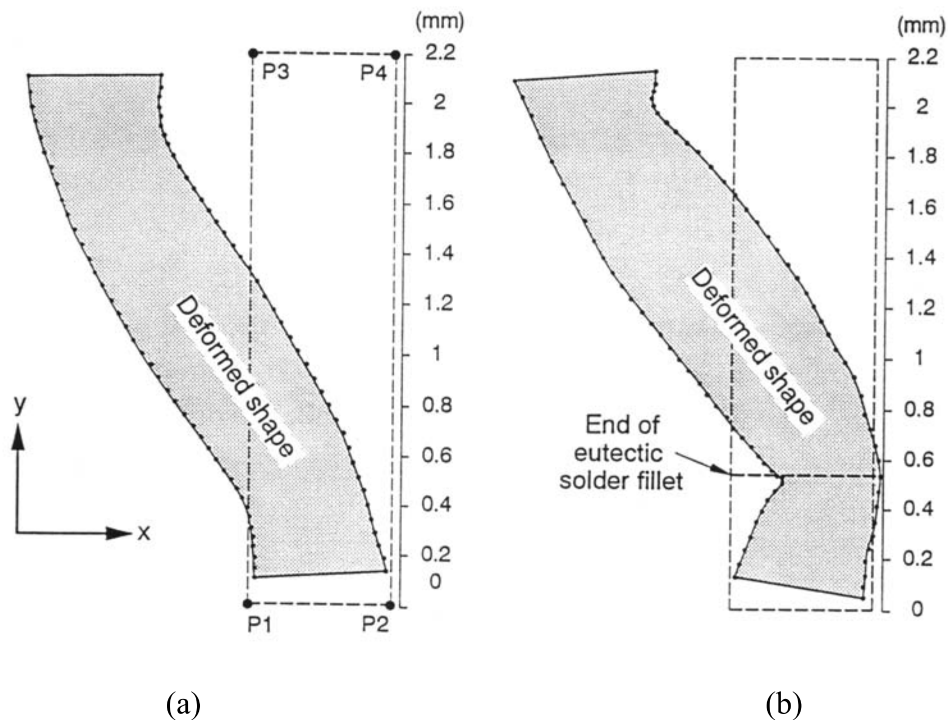

Fig. 10 Deformed shape of solder columns (a) after the initial thermal loading and (b) after four thermal cycles [55]

different temperature dependent properties of the two solder materials are critical parameters for accurate assessment of cycles-to-failure prediction under actual operating conditions.

3.5 Micromechanics: Micro Via in Build-up Structure

One of several purposes of a chip carrier is to provide conducting paths between the extremely compact circuits on the chip and the more widely spaced terminals on the PCB. Recent micro via technology enabled the industry to produce laminate substrates with high density, and fine pitch conductors as required for advanced assemblies. A cross-sectional view of a high-density organic substrate is illustrated in Fig. 11 [68]. Photosensitive dielectric layers (insulators) are built up sequentially with patterned layers of copper plating (typically 25 μm thick).

Extensive research and development efforts have been and are being made to perfect the underfill process for these organic substrates, and to develop optimum underfill materials for the larger silicon devices. An important trend in newly developed underfill materials is its increased Young's modulus, which increases the coupling between the silicon chip and the substrate. This high degree of coupling transfers the CTE mismatch-induced-loading to the build-up layers of the substrate.

Microscopic moiré interferometry was employed to quantify the effect of the underfill on the deformations of the microstructures within the build-up layers [59]. Two specimen configurations were analyzed to study the

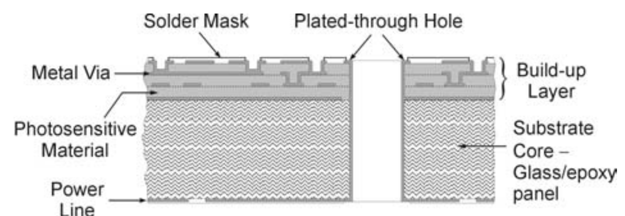

Fig. 11 Schematic diagram of a high-density organic substrate with build-up structures

deformations induced by the subsequent manufacturing process: a bare substrate and a flip chip package. The flip-chip assembly is illustrated schematically in Fig. 12a with its relevant dimensions. In the assembly, a silicon chip was attached to a high-density substrate by solder bumps and the gap between the solder bumps was filled with an underfill.

The specimens were cut and ground to expose the desired microstructures as illustrated schematically in Fig. 2b, where the insert depicts the detailed microstructures within the build-up layer. An epoxy specimen grating was applied at an elevated temperature of 92°C in a small region containing the microstructures. A tiny volume of the epoxy was applied around the region of interest with a sharp-pointed tool and an ULE grating mold was pressed against the epoxy to spread it into a thin film over the region. The fringes were recorded at a room

 S03000 © IMechE 2001

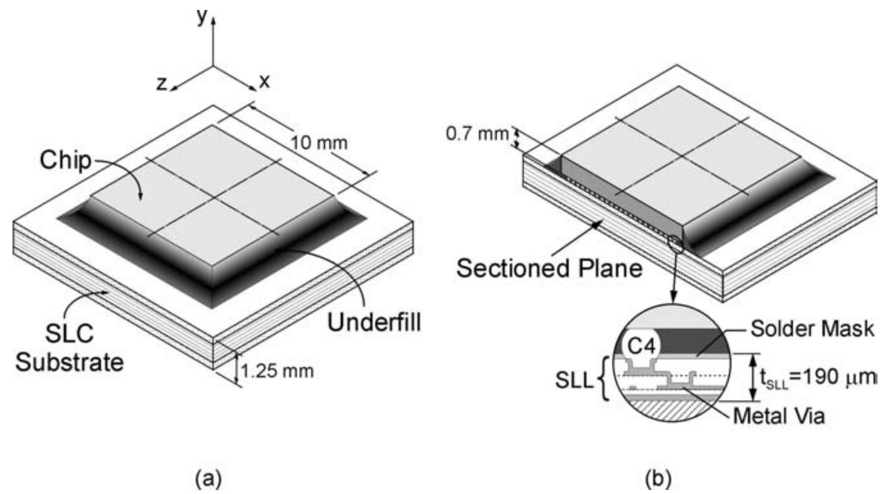

Fig. 12 Schematic diagram of the flip-chip assembly on a high-density substrate (a) before and (b) after specimen preparation

temperature of 22°C, recording the thermal deformation for ΔT = -70°C. The displacement fields for a small region containing the microstructures were recorded by microscopic moiré interferometry. The region is marked by a dashed box in Fig. 13a; it is approximately 500 μm by 375 μm. The resultant fringe patterns are shown in Fig. 13b for the bare substrate and Fig. 13c for the flip-chip assembly. A fringe multiplication factor of $\beta = 4$ was used to produce a displacement contour interval of 52 nm/fringe.

The copper micro vias are imbedded in the build-up layer. The CTE of the copper (17 ppm/°C) is much smaller than the CTE of the photosensitive material (greater than 40 ppm/°C). Consequently, the photosensitive material contracts more than the vias during cooling. Since the photosensitive material is confined by the metal via and the adjacent layer, the different expansion rate causes deformations within the metal vias.

The deformation of a small segment of metal via, CC' (see the insert of Fig. 14), was analyzed to investigate the effect of the chip and underfill. The deformed shape of the portion CC' in the flip chip assembly was evaluated from the fringe patterns in Fig. 13c and the results are plotted in Fig. 14a.

The center portion of CC' is connected rigidly to the solder bump/underfill layer while the left and right segments are extended into the photosensitive material. As can be seen from the deformed shape, these segments moved in the positive y direction (upwards) relative to the center portion. This movement produced a shear strain in the segments, which is plotted in Fig. 14b. The maximum shear strain occurred near the end of the right segment and its magnitude was 0.38 per cent. The shear strain of the same segment in the bare substrate is also plotted in Fig. 14b. The effect of the extra constraint from the solder and underfill layer is evident.

4 TRENDS/PREDICTIONS

Speculation raises mixed emotions. There is the exhilaration of predicting future events, coupled with the uncertainty of foresight. Nevertheless, our view of the trends and developments expected in the next few years is offered.

4.1 Instrumentation

Less complicated designs for moiré and microscopic moiré interferometer system are anticipated. Instruments designed exclusively for transparent replicas will be the least complex, but those offering the greatest versatility will be simplified as well.

Current instruments endeavor to achieve initial null fields. Future implementations may accept several fringes in the initial field, coupled with computer aided means of subtracting them from the final field.

The current trend toward use of CCD cameras instead of film cameras is expected to continue. Emphasis will be placed on variable image magnification so that regions of high fringe density can be resolved by using higher magnifications, and global patterns can be recorded with lower magnifications. A large range of magnifications will be provided to serve a wide variety of applications. Emphasis will be devoted to strong and uniform light

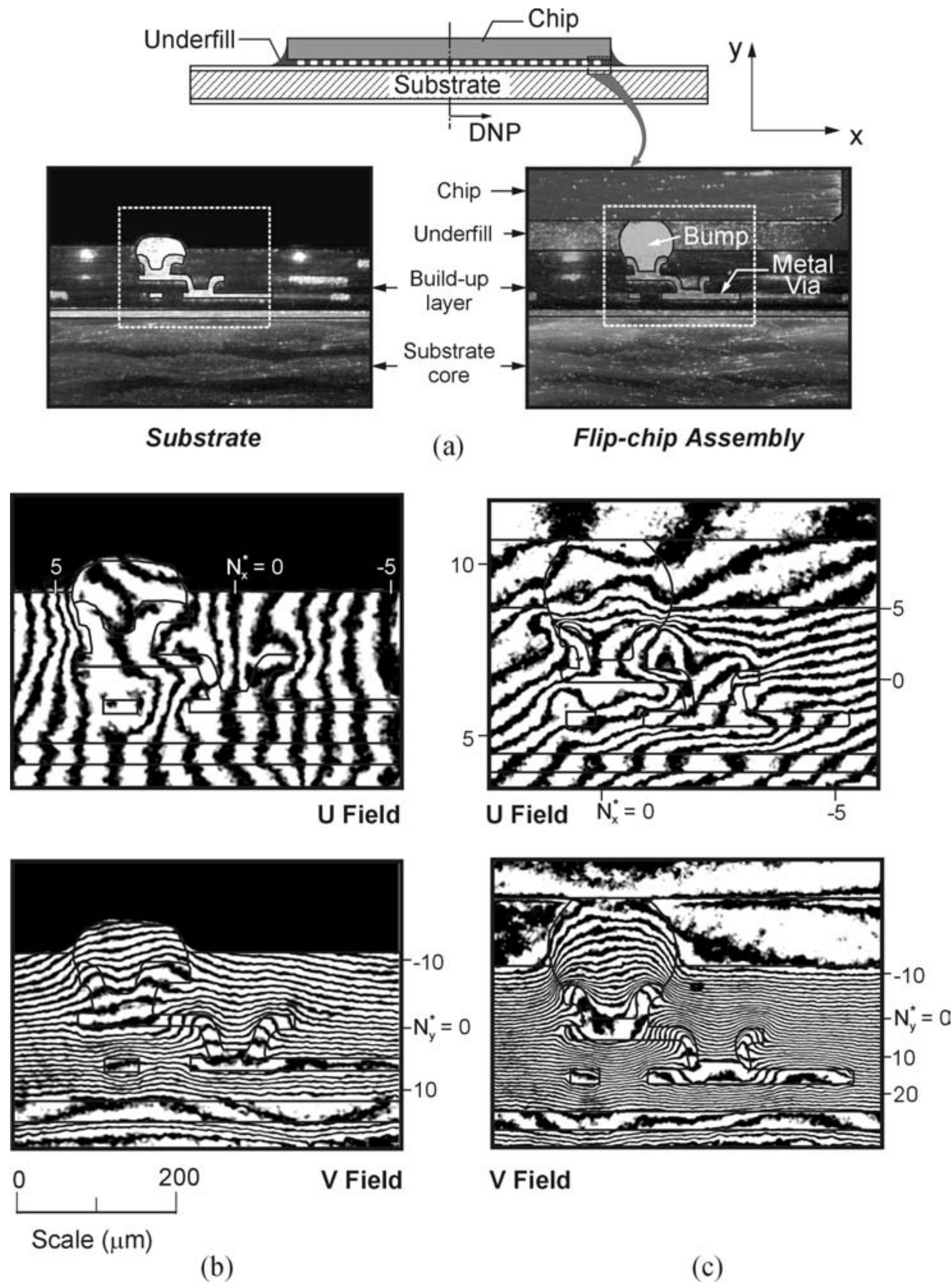

Fig. 13 (a) Micrographs of the region of interest. (b),(c) Microscopic U and V displacement fields of (b) the bare substrate and (c) the flip-chip assembly. The contour interval is 52 nm per fringe [59]

distribution, to achieve high quality fringe patterns at all magnifications.

4.2 Replication of Deformed Gratings

Replication is well known in science and technology. The following examples are seen: in scanning electron microscopy, where details of a specimen surface are reproduced on a small substrate so that it can fit conveniently in the scanning electron microscope; in composite research, where replicas are used for microscopic inspection of fibre and matrix anomalies; in spectrographic grating manufacture, where commercial gratings are copied from very expensive master gratings. Replication is a process of copying details. In our context, the details lie in the deformation of a specimen grating after the specimen is subjected to mechanical loads and/or environmental changes.

Replication has been applied beneficially in a few applications of moiré interferometry. It was used to measure the deformation of an electronic package at a cryogenic temperature [1]. It was used to measure

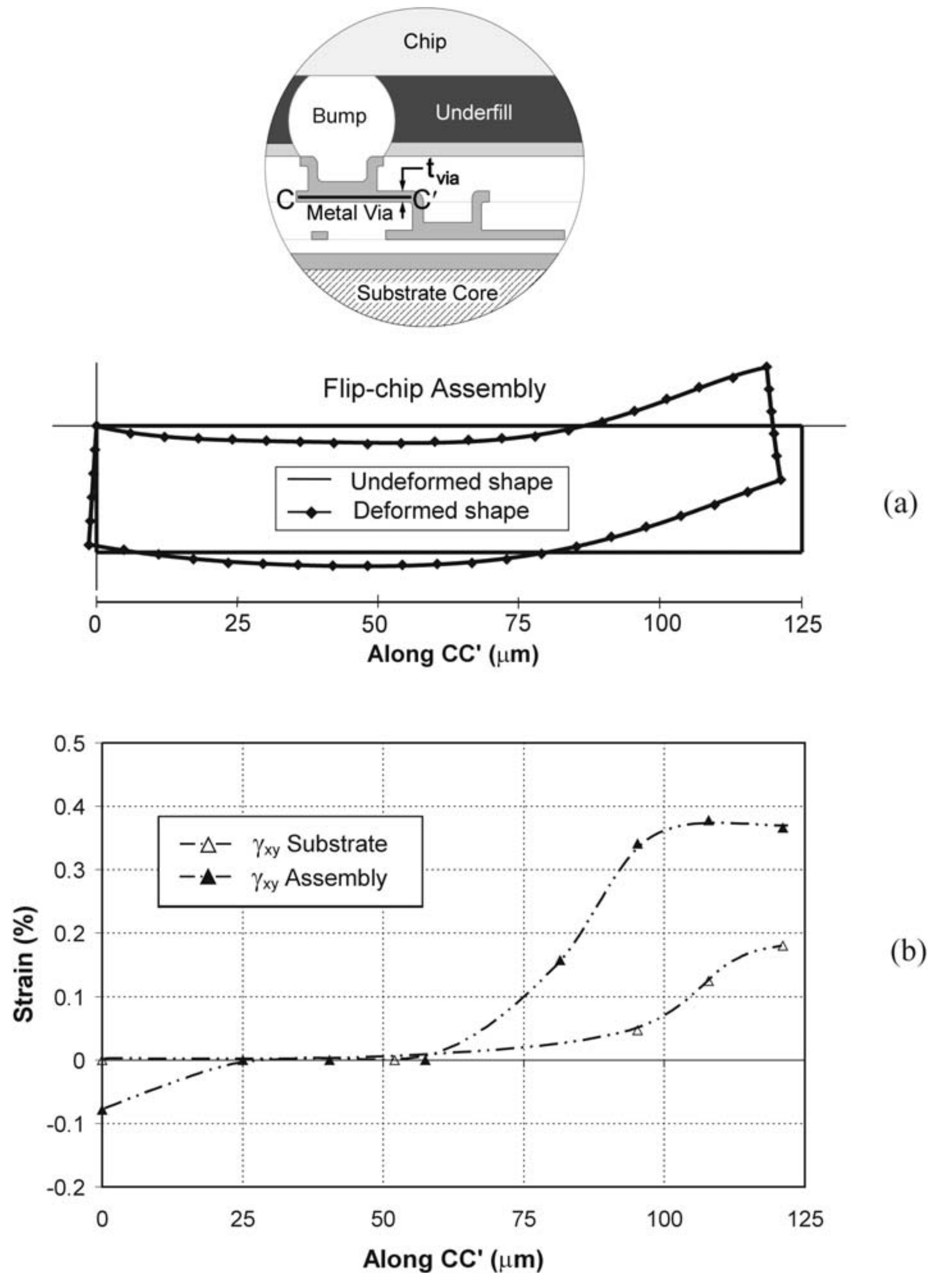

Fig. 14 (a) Deformed shape of the micro via segment CC' in the flip chip assembly and (b) shear strain distribution along CC' [59].

deformations along curved surfaces of composite laminates [11,18]. In a classical paper by McKelvie and Walker [69], replication was advocated for remote sites and harsh environments, followed by analysis of the replicas in the laboratory.

Now, replication is envisaged as a routine practice. In this practice, a grating is applied to the specimen or workpiece in the usual way. Then, the workpiece is subjected to its working loads, e.g. in a mechanical testing machine, which deforms the specimen and the specimen grating. Replicas of the deformed grating are made at desired intervals in the loading process, and subsequently these replicas are analyzed in a moiré interferometer.

Replication provides numerous advantages for typical applications. No limits are applied to the size of the workpiece. Familiar equipment can be used for loading, including large or special-purpose machines. Vibrations and air currents, which otherwise might have to be suppressed for observations with a moiré interferometer, are inconsequential. The technique can be applied conveniently in the field, far from the laboratory, and in difficult environments. In many applications, replicas can be made for cases where the loading is not mechanical, but stems

from changes of temperature, humidity, chemical or radiation environments, etc.

Further advantages accrue for equipment requirements. Loading devices on the optical table are not needed. The replicas can be made on transparent substrates, enabling use of transmission systems of moiré interferometry instead of the current reflection systems. Then, vacuum deposition equipment for applying reflective coatings would not be required. When transmission systems are used, the camera lens can be located very close to the replica, and therefore, very high magnifications become convenient. Additionally, the replicas become permanent records of the deformation, so there is easy recourse to checking and extending an analysis after an initial investigation.

What developments are required? Although the replication method can be practiced with current technology, it would be advantageous to find techniques for quick and routine replication of deformed gratings. This involves optimum combinations of specimen grating materials and quick-setting replication materials; and it involves use of self-releasing grating materials or use of appropriate parting agents to allow easy separation of the replica from the specimen. Such materials are available and systematic investigations will lead to optimized procedures.

4.3 Micromechanics

Extensive use of microscopic moiré interferometry is foreseen for micromechanics studies. Special instrumentation will continue to be developed, consistent with the special requirements of micromechanics applications. Although there is no definite size criterion, the maximum field size will generally be less than a square millimeter, and a range of magnifications will isolate much smaller fields.

Techniques to enhance the measurement sensitivity will be advanced for microscopic moiré interferometry. Since the basic sensitivity depends upon the frequency, f, of the virtual reference grating, further increases of f will be introduced by utilizing light of shorter wavelengths. Ultraviolet light or immersion interferometry, or both, will provide the shorter wavelengths.

The enhancement of basic sensitivity will help, but in most cases the fringe patterns will still be too sparse; the number of fringes in the field will be too small for an accurate analysis. Additional data will be needed and these data will be obtained by phase stepping. The uncertainties introduced by random electronic noise in the CCD camera and associated hardware will be minimized by repeating the measurements a number of times and averaging the results. Alternatively, electronic components of highest performance will be selected. The additional effort and expense would be justified for analyses involving few fringes, in contrast to those that exhibit an abundance of fringes.

The algorithms that transform the fringe data to displacement and strain fields will advance, too. They will become more interactive to allow compensation for local defects or special conditions. The traditional quasi-heterodyne method, which is used most successfully for the inspection of optical surfaces, will be optimized for microscopic moiré interferometry. The optical/digital fringe multiplication method [65] will be extended to produce a larger number of fringe contours from a given number of phase steps.

Also most problems at the finest level of micromechanics (with the small region of interest) will utilize replicas of the deformed grating. Then, transmission-type moiré interferometers will allow the highest magnification and spatial resolution. This scheme provides the greatest stability, and thus, the optimum conditions for phase stepping. In-plane displacements of the order of 1 nm will be measured reliably by microscopic moiré interferometry.

4.4 Data Reduction from Single Images

For most macromechanics analyses, moiré interferometry provides a great number of stress-induced fringes, sufficient for a detailed analysis. Yet, in current practice, there is a tendency to use phase-stepping schemes to reduce these data to graphs of displacement and strain distributions [70-75]. In many cases, the measurements are conducted at abnormally low load levels in order to reduce the number of moiré fringes in the field, since the phase-stepping algorithms are more effective with sparse fringe patterns. This is artificial suppression of data, and the practice seems counterproductive.

The phase-stepping algorithms enjoy popularity mostly because they enable automatic data reduction. However, there are drawbacks that can lead to serious errors. These include electronic noise in the CCD camera, frame grabber, and allied electronics, which contribute random variations to the data—data that might already be suppressed. Stability of the moiré interferometer during the phase-stepping process is crucial, but it can be difficult to ensure sufficient stability under the conditions of some experimental investigations. Automated analyses do not recognize extraneous inputs like those from scratches or other imperfections of the specimen grating. Automated analyses do not cope well with rapidly changing displacement fields, for example, those that can be encountered in composite materials that show differential response of fiber and matrix components. Finally, a common human error should be mentioned; automated analyses must not be allowed to extend across regions of dissimilar materials.

For most practical analyses, quantitative results are extracted at designated locations, i.e. at points, or along lines in the specimen. It is significant to observe the nature of the data reduction in the three real-world industrial analyses reviewed above. As is usual, the analyses were designed to investigate specific characteristics of the structure. Quantitative data were extracted at key locations (center-lines and boundary points in these cases) and whole-field analysis techniques were not employed.

Thus, for the majority of applications (those that exhibit numerous fringes) another scheme of data reduction would be beneficial. New schemes of computer aided analysis will be developed that produce displacement and strain

 S03000 © IMechE 2001

graphs from a single pair of moiré fringe patterns, i.e., single images of the U and V fields. They will likely require user input, firstly to choose regions of interest and to determine whether carrier fringes should be used in these regions; and secondly, to deal with possible imperfections in the fringe patterns, such as those from scratches in the gratings. The computer techniques will probably quantify the locations of fringes and graph displacement fields from these; apparent displacement from carrier fringes would be subtracted off. Strains would be calculated from computer measurements of the x and y components of distance between fringes (the distance either between neighboring fringes or between more distant fringes); the operator would decide. A variety of algorithms that reduce tedious aspects of the analyses but retain the logical step-by-step human input that is present in manual analyses could be developed.

Fourier methods utilize single fringe patterns and they offer current alternatives to phase-stepping analyses. However, they do not offer the high fidelity and user discretion and control that may be desired. As the technology evolves, a Fourier technique may be employed for a global view of the strain field, followed by a direct computer aided analysis for local regions of special interest. The key will be human understanding and control, replacing relatively blind automation.

4.5 Applications

Moiré and microscopic moiré interferometry have become extremely important tools in the electronics industry for electronic packaging studies. Their application (mostly to evaluate thermal strains, but also for mechanical loading and material characterization) is introduced at design and development, evaluation, and process control stages. Applications for the study of composite materials and components are extensive and increasing, but not yet rivaling the electronics packaging activity. Other areas of strong and growing interest include fracture mechanics, biomechanics, rheology of plastics, metallurgy and ceramic science. Both the scope and volume of analyses are growing together with the ever more complex developments in engineering and science, and in juxtaposition and support of the ever more complex analyses by numerical computer studies.

4.6 Propagation into College/University Curricula

It is predicted that the theory and practice of moiré interferometry will be taught at most colleges in engineering, science, and technology curricula. The method will be introduced in physics courses (lecture and laboratory) as a practical application of optics and interferometry. It will be introduced in traditional mechanics of materials courses to visualize and measure load-induced deformations. The method will be studied in more depth in courses on optics for engineering and science; and it will be studied most comprehensively in stand-alone courses on moiré interferometry.

Instrumentation will become available for these educational purposes, and it will be more basic and economical. Transmission systems used with replicas might become typical for demonstrations and exercises. As the technology propagates, it is likely that new innovative designs will emerge. The more advanced courses will surely encounter computer aided analysis. These experiences will inevitably lead to experimentation with alternate schemes of analysis, and superior programs will evolve.

We believe this propagation will occur in the next decade, and moiré interferometry will become familiar in engineering and science. It will be known by many as a tool for measurement and exploration.

ACKNOWLEDGEMENTS

Portions of this article are excerpted with permissions from chapters by the same authors in two books: P. K. Rastogi (Ed.), Photomechanics, 1999 (Springer-Verlag, Berlin); P.K. Rastogi and D. Inaudi (Eds), Trends in Optical Nondestructive Testing and Inspection, 2000 (Elsevier, Amsterdam). The authors extend thanks to the publishers.

REFERENCES

1 **Post, D., Han, B.** and **Ifju, P.** High Sensitivity Moiré: Experimental Analysis for Mechanics and Materials, 1994 (Springer-Verlag, New York).

2 **McDonach, A., McKelvie, J.** and **Walker, C.A.** Stress analysis of fibrous composites using moiré interferometry, *Optics Lasers Engng*, 1980,**1**(2), 185-205.

3 **Hyer, W. M., Herakovich, C. T.** and **Post, D.** Thermal expansion of graphite epoxy. In *1982 Advances in Aerospace Structures and Materials*, 1982, pp. 107-114, (American Society of Mechanical Engineering, New York).

4 **Wood, J. D.** Detection of Delamination onset in a composite laminate using moiré interferometry *Composite Technol. Rev.*, 1985, **7**(4), 121-128

5 **Tuttle, M. E.** and **Klein, R. J.** Compressive creep strain measurements using moiré interferometry," *Opt Engng*, 1988, **27**(8), 630-635.

6 **Post, D., Morton, J., Wang, Y.** and **Dai, F. L.** Interlaminar compression of a thick composite. In Proceedings of the Fourth Annual Meeting of the American Society for Composites, 1989, pp.101-106.

7 **Post, D., Guo, Y.** and **Czarnek, R.** Deformation analysis of boron/aluminum specimens by moiré interferometry. In *Metal Matrix Composites: Testing Analysis, and Failure Modes,* ASTM STP 1032 (Ed. W.S. Johnson), 1989, pp. 161-170 (American Society for Testing and Materials, Philadelphia, Pennsylvania).

8 **Post, D.** Moiré interferometry for composites. In *Manual on Experimental Methods for Mechanical Testing of Composites*

(Eds R.L. Pendleton and M.E. Tuttle), 1989, pp. 67-80 (Society for Experimental Mechanics, Bethel, Connecticut)

9 **Tuttle, M. E.** and **Graesser, D. L.** Compression creep of graphite/epoxy laminates monitored using moiré interferometry," *Optics Lasers Engng*, 1990, **12**(2), 151-172.

10 **Gascoigne, H. E.** and **Abdallah, M. G.** Strain analysis of a bonded dissimilar, composite material T-Joint using moiré interferometry. *Optics Lasers Engng*, 1990, **13**, 155-165.

11 **Boeman, R. G.** Interlaminar deformations on the cylindrical surface of a hole in laminated composites: an experimental study. Center for Composite Materials and Structures Report 91-07, Virginia Polytechnic Institute and State University, Blacksburg, Virginia, 1991.

12 **Gascoigne, H. E.** and **Abdallah, M. G.** Displacements and strains in thick-walled composite rings subjected to external pressure using moiré interferometry. In Proceedings of 2nd International Conference on *Photomechanics* and *Speckle Metrology*, Proceedings of the SPIE, Vol. 1554B, 1991, pp. 315-322 (Society of Photo-optical Instrumentation Engineers, Bellingham, Washington)

13 **Guo, Y., Post, D.** and **Han, B.** Thick composites in compression: an experimental study of micromechanical behavior and smeared engineering properties. *J. Composite Mater.,* 1992, **26**(13), 1930-1944.

14 **Masters, J. E., Fedro, M. J.,** and **Ifju, P. G.** Experimental and analytical characterization of triaxially braided textile composite materials. In Proceedings of Third NASA Advanced Composites Technology Conference, NASA CP-3178, Long Beach, California, 1992, pp. 263-285.

15 **Ifju, P. G., Masters, J. E.,** and **Jackson, W.C.** Using moiré interferometry to aid in standard test method development for textile composite materials. *Composites Sci. Technol.,* 1995, **53**, 155-163.

16 **Ifju, P. G.** Shear testing of textile composite materials *ASTM J. of Composites Technol. Res.*, July 1995, **17**(3), 199-204

17 **Rhee, J., He, S.** and **Rowlands, R. E.** Hybrid moiré-numerical stress-analysis around cutouts in loaded composites. *Expl Mechanics*, 1996, **36**, 379-387.

18 **Mollenhauer, D. H.** Interlaminar deformation at a hole in laminated composites: a detailed experimental investigation using moiré interferometry. Ph.D. Dissertation, Virginia Polytechnic Institute and State University, Blacksburg, Virginia, 1997; Available for download at http://scholar.lib.vt.edu/theses/theses.html

19 **Han, B.** Micromechanical deformation analysis of beta alloy titanium in elastic and elastic/plastic tension. *Expl Mechanics*, 1996, **36**, 120-126.

20 **Park, S. B., Park, S. S., Carman, G. P.** and **Hahn, H. T.** Measuring strain distribution during mesoscopic domain reorientation in a ferroelectric material. *J. Engng Mater. Technol.*, 1998, **120**, 1-6.

21 **Post, D., Czarnek, R.** and **Smith, C. W.** Patterns of *U* and *V* displacement fields around cracks by moiré interferometry. In *Application of Fracture Mechanics to Materials and Structures* (Eds G. C. Sih, E. Sommer and W. Dehl), 1984, pp.699-708 (Martinus Nijhoff, Boston, Massachusetts)

22 **Smith, C. W.** Measurements of three-dimensional effects in fracture mechanics. In *Fracture Mechanics* (19th Conference), ASTM STP 969, 1988, pp. 5-18 (American Society for Testing and Materials, Philadelphia, Pennsylvania).

23 **Dadkhah, M. S.** and **Kobayashi, A. S.** HRR field of a moving crack, an experimental analysis. *Engng Fracture Mechanics*, 1989, **34**, 253-262.

24 **Nicoletto, G.** Moiré interferometric fringe patterns about crack tips: experimental observations and numerical simulations. *Optics Lasers Engng*, 1990, **12**(2), 135-150.

25 **Epstein. J. S., Jung, H. Y.** and **Reuter, W. G.** Stress intensity factor extraction using moiré interferometry based on a 2-parameter displacement eigenfunction-validity criteria and comparison with ASTM E-399 K_{Ic} plane strain test methods. *Optics Lasers Engng*, 1990, **13**, 167-180.

26 **Epstein, J. S.** and **Dadkhah, M. S.** Moiré interferometry in fracture mechanics. In *Experimental Techniques in Fracture*, Vol. III, (Ed. J.S. Epstein), 1993, pp. 427-508 (VHC Publishers, New York).

27 **Poon, C. Y.** and **Ruiz, C.** Hybrid experimental-numerical approach for determining strain-energy release rates. *Theor. Appl. Fracture Mechanics*, 1994, **20**, 123-131.

28 **Perry, K. E.** and **McKelvie, J.** Measurement of energy release rates for delaminations in composite materials *Expl Mechanics*, 1996, **36**, 55-63.

29 **Wood, J. D., Wang, R. Z., Weiner, S.** and **Pashley, D. H.** Mapping of deformation caused by moisture change using moiré interferometry. Dent. Mater., May 1999 (submitted).

30 **Walker, C. A., McDonach, A., MacKenzie, P.** and **McKelvie, J.** Dynamic moiré measurement of strains induced in a titanium tube plate during rolling of a series of tubes. *Expl Mechanics*, 1985, **25**(1), 1-5.

31 **Morton, J., Post, D., Han, B.** and **Tsai, M. Y.** A localized hybrid method of stress analysis: a combination of moiré interferometry and FEM. *Expl Mechanics*, 1990, **30**(2), 195-200.

32 **Czarnek, R.** and **Post, D.** Moiré interferometry with ±45° gratings applied to the dovetail joint. In Proceedings of 1985 SEM Spring Conference on *Experimental Mechanics*, 1985, pp. 553-559 (Society for Experimental Mechanics, Bethel, Connecticut).

33 **Chavez, S. A., Deason, V. A.** and **Epstein, J. S.** Use of moiré interferometry in weldments. In Proceedings of International Conference on *Trends in Welding Research* (Ed. S. A. David), 1986, pp. 533-537 (American Society for Metals, Metals Park, Ohio).

34 **Post, D., Czarnek, R., Wood, J. D.** and **Joh, D.** Deformations and strains in a thick adherend lap joint. In *Adhesively Bonded Joints: Testing, Analysis and Design*, ASTM STP 981 (Ed. W. S. Johnson), 1988, pp. 107-118 (American Society for Testing and Materials, Philadelphia, Pennsylvania).

35 **Post, D., Wood, J. D., Han, B., Parks, V. J.** and **Gerstle Jr, F. P.** Thermal stresses in a bimaterial joint: an experimental analysis. *J. Appl. Mechanics*, 1994, **61**(1), 192-198.

36 **Joh, D., Byun, K. Y.** and **Ha, J.** Thermal residual stresses in thick graphite/epoxy composite laminates-uniaxial approach *Expl Mechanics*, 1993, **33**, 70-76.

37 **Gascoigne, H.** Residual surface stresses in laminated cross-ply fiber-epoxy composite materials. *Expl Mechanics*, 1994, **34**, 27-36.

38 **Nicoletto, G.** Theoretical fringe analysis for a coherent optics method of residual stress measurement. *J. Strain Analysis*, 1988, **23**, 169-178.

39 **Nicoletto, G.** Moiré interferometry determination of residual stresses in the presence of gradients. *Expl Mechanics*, 1991, **31**(3), 252-256.

40 **Wu, Z., Lu, J.** and **Han, B.** Study of residual stress distribution by a combined method of moiré interferometry and incremental hole drilling. Part I: theory. *J. Appl. Mechanics*, 1998, **65**, 837-843.

41 **Wu, Z., Lu, J.** and **Han, B.** Study of residual stress distribution by a combined method of moiré interferometry

and incremental hole drilling. Part II: implementation. *J. Appl. Mechanics*, 1998, **65**, 844-850.

42 **Ifju, P., Niu, X., Kilday, B., Liu, S.-C.** and **Ettinger, S.** Residual strain measurement in composites using the cure-referencing method. *Expl Mechanics*, 2000, **40**(1), 22-30.

43 **Watson, R. B.** and **Post, D.** Precision strain standard by moiré interferometry for strain gage calibration. *Expl Mechanics*, 1982, **22**(7), 256-261.

44 **Bastawros, A. F.** and **Voloshin, A. S.** Transient thermal strain measurements in electronic packages. *IEEE Trans. Components, Hybrids and Mfg Technol.*, 1990, **13**(4), 961-966.

45 **Bastawros, A. F.** and **Voloshin, A. S.** *In situ* calibration of stress chips. *IEEE Trans. on Components, Hybrids and Mfg Technol.*, 1990, **13**(4), 888-892.

46 **Bastawros, A. F.** and **Voloshin, A. S.** Thermal strain measurements in electronic packages through fractional fringe moiré interferometry. *Trans. ASME, J. Electronic Packaging*, 1990, **112**(4), 303-308.

47 **Guo, Y., Chen, W. T.** and **Lim, C. K.** Experimental determination of thermal strains in semiconductor packaging using moiré interferometry. In Proceedings of 1992 Joint ASME-JSME Conference on *Electronic Packaging*, 1992, pp.779-784 (American Society of Mechanical Engineers, New York).

48 **Wu, T. Y., Guo, Y.** and **Chen, W. T.** Thermal-mechanical strain characterization for printed wiring boards *IBM J. Res. Dev.*, 1993, **37**(5), 621-634.

49 **Guo, Y., Lim, C. K., Chen, W. T.** and **Woychik, C. G.** Solder ball connect (SBC) assemblies under thermal loading. I: deformation measurement via moiré interferometry, and its interpretation. *IBM J. Res. Dev.*, 1993, **37**(5), 635-648.

50 **Han, B.** and **Guo, Y.** Thermal deformation analysis of various electronic packaging products by moiré and microscopic moiré interferometry. *Trans. ASME, J. Electronic Packaging*, 1995, **117**, 185-191.

51 **Tsao, P. H.** and **Voloshin, A. S.** Manufacturing stresses in the die due to die-attach process. *IEEE Trans. Components, Packaging Mfg Technol. A*, 1995, 18(1), 201-205.

52 **Han, B., Guo, Y., Lim, C. K.** and **Caletka, D.** Verification of numerical models used in microelectronics packaging design by interferometric displacement measurement methods. *Trans. ASME, J. Electronic Packaging,* 1996, **118**, 157-163.

53 **Han, B.** and **Guo, Y.** Determination of effective coefficient of thermal expansion of electronic packaging components: a whole-field approach. *IEEE Trans. Components, Packaging Mfg Technol. A*, 1996, **19**(2), 240-247.

54 **Han, B., Chopra, M., Park, S., Li, L**. and **Verma, K.** Effect of substrate CTE on solder ball reliability of flip-chip PBGA package assembly. *J. Surf. Mount Technol.*, 1996, **9**, 43-52.

55 **Han, B.** Deformation mechanism of two-phase solder column interconnections under highly accelerated thermal cycling condition: an experimental study. *Trans. ASME, J. Electronic Packaging*, 1997, **119**, 189-196.

56 **Han, B. and Guo, Y.** Photomechanics tools as applied to electronic packaging product development. In *Experimental/ Numerical Mechanics in Electronics Packaging*, Vol. 1 (Eds B. Han, R. Mahajan and D. Barker), 1997, pp. 11-15 (Society for Experimental Mechanics, Bethel, Connecticut).

57 **Han, B.** Recent advancement of moiré and microscopic moiré interferometry for thermal deformation analyses of microelectronics devices. *Expl Mechanics*, 1998, **38**(4), 278-288.

58 **Voloshin, A. S., Tsao, P. H.** and **Pearson, R. A.** *In situ* evaluation of residual stresses in an organic die-attach adhesive. *Trans. ASME, J. Electronic Packaging*, 1998, **120**(3), 314-318.

59 **Han, B.** and **Kunthong, P.** Micro-mechanical deformation analysis of surface laminar circuit in organic flip-chip package: an experimental study *Trans. ASME, J. Electronic Packaging*, 2000, **122**(4), 294,300.

60 **Patorski, K.** *Handbook of the Moiré Fringe Techniques*, 1993 (Elsevier, New York).

61 **Cloud, G.** *Optical Methods of Engineering Analysis*, 1995 (*Cambridge University Press*, Cambridge).

62 **Livnat, A.** and **Post, D.** The governing equations of moiré interferometry and their identity to equations of geometric moiré. *Expl Mechanics*, 1985, **25**(4), 360-366.

63 **Mollenhauer, D. H., Ifju, P.** and **Han, B.** A compact, robust, and versatile moiré interferometer. *Optics Lasers Engng*, 1995, **23**(1), 29-40.

64 **Han, B.** and **Post, D.** Immersion interferometer for microscopic moiré interferometry. *Expl Mechanics*, 1992, **32**(1), 38-41.

65 **Han, B.** Interferometric methods with enhanced sensitivity by optical/digital fringe multiplication. *Appl. Optics*, 1993, **32**(25), 4713-4718.

66 **Han, B.** Higher sensitivity moiré interferometry for micromechanics studies. *Opt. Engng*, 1992, **31**(7), 1517-1526.

67 **Post, D.** and **Wood, J.** Determination of thermal strains by moiré interferometry. *Expl Mechanics*, 1989, **29**(3), 318-322.

68 **Tsukada, Y.** Solder bumped flip chip attach on SLC board and multi-chip module. in *Chip on Board* (Ed. J. H. Lau), 1994, Ch. 9, pp. 410-443 (Van Nostrand Reinhold, New York).

69 **McKelvie, J.** and **Walker, C. A.** A practical multiplied moiré-fringe technique. *Expl Mechanics*,1978,**18**(8), 316-320.

70 **Hariharan, P.** Quasi-heterodyne hologram interferometry. *Opt. Engng*, 1985, **24**(4), 632-638.

71 **Dandliker, R.** and **Thalmann, R.** Heterodyne and quasi-heterodyne holographic interferometry. *Opt. Engng*, 1985, **24**(5), 824-831.

72 **Brownell, J. B.** and **Parker, R. J.** Automated fringe analysis for moiré interferometry. In Proceedings of 2nd International Conference on *Photomechanics* and *Speckle Metrology*, Proceedings of the SPIE, Vol. 1554B, 1991, pp 481-492 (Society of the Photo-optical Instrumentation Engineers, Bellingham, Washington).

73 **Poon, C. Y., Kujawinska, M.** and **Ruiz, C.** Automated fringe pattern analysis for moiré interferometry. *Expl Mechanics*, 1993, **33**, 234-240.

74 **Perry, K. E.** and **McKelvie, J.** A comparison of phase shifting and Fourier methods, in the analysis of discontinuous fringe patterns. *Optics Lasers in Engng*, 1993, 19, 269-284.

75 **Huntley, J. M.** Automated fringe pattern analysis in experimental mechanics: a review. *J. of Strain Analysis*, 1998, **33**, 105-126.